ORIGINAL ARTICLE

lajss.org© Latin American Journal of Solids and Structures

www.lajss.org

Stage-wise analytical modeling and full-scale validation of TRC-strengthened RC beams under sustained loading: application to 30-year-old bridge members

Huy Cuong Nguyen[a], Dang Dung Le[a], Van Hiep Vu[a], Cong Hau Nguyen[a], Thi Thanh Mai Bui[a*]

[a]University of Transport and Communications, No.3 Cau Giay Street, Hanoi, Vietnam. Email: nguyenhuycuong@utc.edu.vn, ledangdung@utc.edu.vn, vvhiep@utc.edu.vn, haunc_ph@utc.edu.vn, bttmai@utc.edu.vn

* Corresponding author

https://doi.org/10.1590/1679-7825/e9053

Abstract

This study presents a stage-wise sectional analytical model for reinforced concrete (RC) beams strengthened with carbon textile-reinforced concrete (TRC) under sustained loading. The formulation accounts for pre-cracking, partial unloading, residual curvature, and TRC activation under non-zero initial strain. The TRC layer is modeled with bilinear tensile behavior, while tension stiffening and residual tensile effects of cracked concrete are included. The model is validated using full-scale bridge beams after about 30 years of service, tested under realistic conditions. The strengthened beam shows an increase of about 25% in ultimate load and improved crack control, with crack width and spacing reduced to one-third to one-half of the control beam. Strain results confirm effective stress redistribution and high textile utilization. Predictions agree well with experiments, with discrepancies within 5–10%. Compared with design guidelines, Z-31.10-182 is closest, while ACI 549.4R-20 and CNR-DT 215/2018 overestimate capacity. The model provides a reliable framework for assessing TRC-strengthened RC members under realistic conditions.

Keywords

Textile-reinforced concrete; Sustained loading; Analytical flexural model; Moment–curvature; Pre-cracked RC beams; Bridge rehabilitation

Graphical Abstract

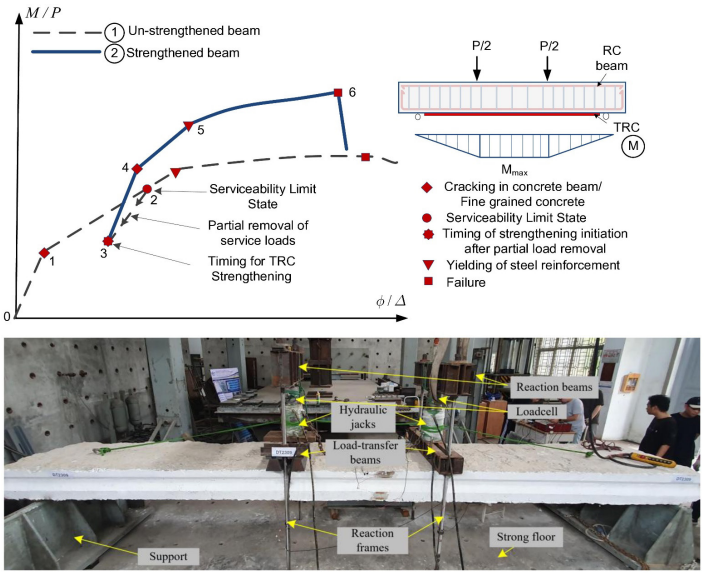

Received March 27, 2026. In revised form April 27, 2026. Accepted April 29, 2026. Available online May 04, 2026.
https://doi.org/10.1590/1679-7825/e9053

1 INTRODUCTION

The rehabilitation of aging reinforced concrete (RC) structures has become an increasingly important engineering task, particularly for bridge members subjected to sustained service loading, environmental deterioration, and progressive cracking. Externally bonded strengthening systems have been widely adopted to restore structural performance, including fiber-reinforced polymer (FRP) composites and textile-reinforced concrete (TRC) systems. Compared with FRP, TRC offers improved compatibility with concrete substrates, enhanced fire resistance, and more distributed crack control behavior, as highlighted in the state-of-the-art review by Koutas et al. (2019) and the synthesis by Bencardino et al. (2018).

Recent studies have demonstrated the effectiveness of TRC and related composite systems in improving flexural performance. Silva et al. (2025) reported significant increases in stiffness and load capacity of RC beams strengthened with mineral-impregnated TRC layers. Adam et al. (2020) showed that TRC strengthening effectively enhances both flexural and shear resistance of bridge deck slabs. Similarly, Wang et al. (2025a) observed that composite strengthening layers combining ultra-high-performance concrete, steel mesh, and carbon textile significantly improve stiffness and delay crack propagation under sustained loading conditions.

In parallel, strengthening techniques based on FRP or hybrid systems have also been widely investigated. Tan et al. (2009) reported that FRP-strengthened beams subjected to sustained loading and environmental exposure exhibit increased deflection and crack width, together with reduced ductility. Guo et al. (2025) demonstrated that pre-damaged RC beams strengthened with FRP grid–ECC composites under sustained loading show significant gains in load capacity, but also exhibit delayed strain development in the strengthening layer. Their analytical model, however, is primarily based on sectional equilibrium to predict ultimate flexural capacity, and does not explicitly capture the full load–deformation response or stage-wise stiffness evolution. Comparative studies by Sabzi et al. (2024) further indicated that TRC systems provide improved compatibility and crack control compared with FRP, although differences in stiffness evolution and failure modes remain significant.

In practical applications, RC members to be strengthened are rarely in an undamaged or unloaded state. Instead, they are typically pre-cracked, may exhibit corrosion damage, and are often subjected to sustained service loads during strengthening. Experimental investigations by Elghazy et al. (2017) and Xie et al. (2023) confirmed that corrosion and pre-existing damage significantly alter the flexural response and failure mechanisms of strengthened beams. Full-scale studies on aged bridge members by Yang et al. (2023) further showed that the effectiveness of strengthening systems strongly depends on the initial damage state and crack distribution.

At the material level, the tensile behavior of TRC systems is inherently composite and multi-stage. Nerilli and Ferracuti (2022) developed a tension stiffening model for TRC reinforcements, showing that post-cracking behavior is governed by matrix cracking and textile bridging rather than purely elastic fiber response. These findings indicate that TRC should be modeled as a composite material with bilinear tensile behavior and distributed cracking mechanisms.

Despite these advances, current design approaches remain limited. Existing guidelines such as ACI 549.4R-20 (ACI, 2020), Zulassung Z-31.10-182 (DIBt , 2023) and CNR-DT 215/2018 (CNR, 2018) provide practical recommendations for TRC strengthening, but generally assume unloaded substrates and do not explicitly consider residual curvature, sustained loading during strengthening, or staged activation of the strengthening layer. Moreover, many analytical models neglect key mechanisms such as tension stiffening of cracked concrete, residual tensile stresses, and non-zero initial strain in the strengthening system.

Therefore, a significant research gap remains. Existing analytical models have been primarily developed and validated on laboratory-scale specimens, typically newly cast or artificially pre-damaged members with limited span length. There is currently no unified analytical framework that simultaneously accounts for (i) pre-cracking and residual curvature prior to strengthening, (ii) sustained service loading during strengthening, (iii) the composite and bilinear tensile behavior of TRC, and (iv) tension stiffening effects in the cracked concrete substrate. More importantly, no study has systematically validated such a model against real, in-service structural members that have undergone long-term natural aging, deterioration, and realistic loading histories. In practical engineering conditions, bridge members are characterized by large spans, accumulated damage over decades of service, and complex residual stress–strain states resulting from sustained loading and environmental exposure. However, experimental evidence on full-scale, naturally aged RC structures remains extremely limited, and the applicability of existing models to such conditions is still unclear.

The objective of this study is therefore to develop a closed-form, strain-controlled, stage-wise sectional analytical model for RC beams strengthened with TRC under sustained loading. The proposed formulation incorporates nonlinear concrete compression, bilinear steel behavior, composite TRC tensile response, residual tensile mechanisms in cracked concrete, and partial unloading prior to strengthening.

In addition, the proposed model is validated against full-scale reinforced concrete bridge slab beams that have been in service for approximately 30 years, representing naturally aged and pre-damaged structural members. The experimental program is designed to replicate realistic field conditions, including sustained loading, pre-existing cracking, and strengthening procedures applied under service states. To the authors' knowledge, very limited studies have investigated the flexural behavior of TRC-strengthened RC members using full-scale, long-span bridge elements subjected to natural aging and realistic strengthening scenarios. By explicitly incorporating sustained-load effects, residual strain states, and composite tensile mechanisms, and by validating the model against real in-service structures, the present study provides a rational and practically relevant mechanical framework for predicting stiffness evolution, yield transition, and ultimate capacity of strengthened RC members.

2 DEVELOPMENT OF CALCULATION MODEL FOR FLEXURAL BEHAVIOR OF TRC-STRENGTHENED RC BEAMS

2.1 Working Stages of the Strengthened RC Beam

The flexural response of TRC-strengthened reinforced concrete (RC) beams under sustained loading is described using a stage-wise analytical framework, in which the behavior is divided into a sequence of distinct mechanical stages (Figure 1). Each stage corresponds to a change in cracking state, stiffness, and internal force redistribution. At low load levels (Stage I), the section remains uncracked and behaves elastically. The flexural response is governed by the gross sectional stiffness, with both concrete (in compression and tension) and steel reinforcement contributing to load resistance. When the tensile stress reaches the concrete cracking strength (Stage II), flexural cracks initiate, leading to a reduction in stiffness and a redistribution of internal forces within the section. Prior to strengthening (Stage III), the beam is partially unloaded. However, the cracks formed during previous loading remain open, and residual curvature persists. As a result, the structural response at the onset of strengthening is characterized by a non-zero residual strain state rather than an unloaded condition.

After TRC application and subsequent reloading (Stage IV), the strengthening layer initially behaves elastically and provides additional tensile resistance. This leads to an increase in the effective stiffness of the cracked section. When the tensile strain in the TRC layer exceeds its cracking threshold (Stage V), matrix cracking occurs within the composite layer, and the response becomes governed by textile bridging and composite interaction. At higher load levels (Stage VI), the tensile steel reinforcement may yield, and the structural response is governed by strain compatibility and progressive stiffness degradation. Ultimate capacity is reached when one of the governing limit states occurs, including concrete crushing, textile rupture, or debonding of the TRC layer.

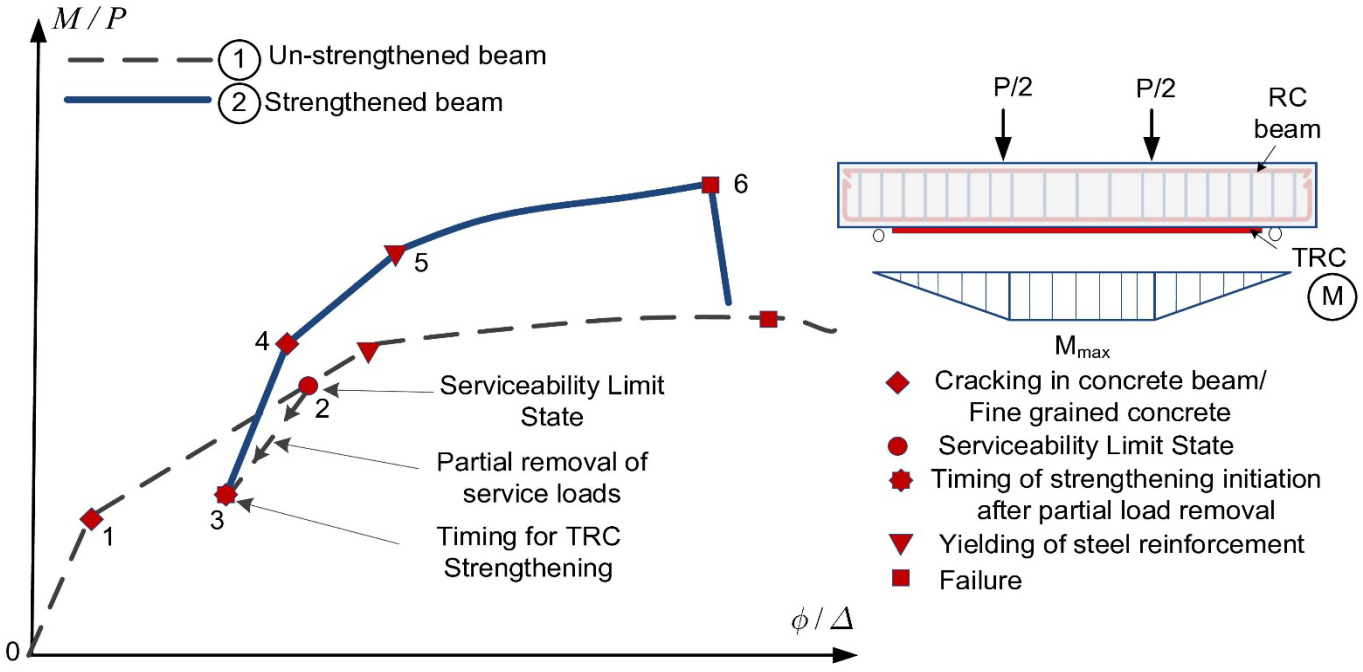

Figure 1 Bending moment–curvature or load–deflection relationship of TRC-strengthened RC beams

2.2 Fundamental Assumptions and Notation

2.2.1 Mechanical assumptions

Plane sections are assumed to remain plane, and full strain compatibility is enforced between the concrete, steel reinforcement, and the externally bonded TRC layer up to the onset of debonding. Concrete in compression follows a nonlinear stress–strain relationship with an ultimate strain of $\varepsilon_{cu} = 0.003$, while steel reinforcement is modeled as elastic–perfectly plastic. The TRC layer is treated as a composite tensile layer with perfect bond between textile and fine-grained matrix. The ultimate state is governed by the earliest occurrence of either concrete crushing or interfacial debonding of the TRC layer. Debonding is assumed to occur when the tensile strain in the TRC reaches a limiting value of approximately 12‰, representing the deformation capacity of the interface–anchorage system. Textile rupture is checked only as an upper bound and does not govern when the debonding strain limit is reached first.

2.2.2 Geometric definitions

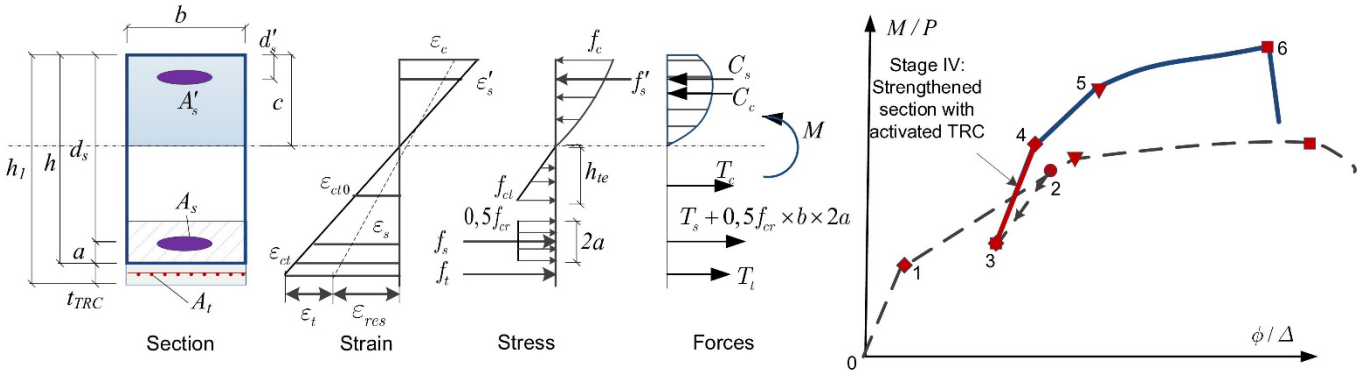

Figure 2 Deformation state of the cross section at stage 3-4 (when the fine-grained concrete is not cracked)

As displayed in Figure 2, a rectangular cross-section of width b and total depth h is considered.

- c: depth of the neutral axis measured from the extreme compression fibre
- d: effective depth of tensile steel reinforcement
- d': depth of compression reinforcement (if present)
- d_{trc}: effective depth of the TRC layer
- A_s, A'_s: areas of tensile and compression steel reinforcement
- A_t: effective tensile area of the TRC layer
- a: characteristic half-spacing defining the local tension-stiffening zone around the tensile reinforcement
- f_{cr}: tensile cracking strength of concrete
- h_{te}: effective height of remaining tensile concrete between cracks

2.2.3 Kinematic relations

Let curvature be denoted by ϕ. The strain at the extreme compression fibre is ε_c. From the plane-section assumption:

$$\phi = \frac{\varepsilon_c}{c} \tag{1}$$

The corresponding strain in the tensile steel reinforcement is:

$$\varepsilon_s = \phi(d - c) \tag{2}$$

The strain in the compression steel reinforcement is:

$$\varepsilon_s' = \phi(c - d') \tag{3}$$

For the TRC layer:

$$\varepsilon_t = \phi(d_{trc} - c) + \varepsilon_{res} \tag{4}$$

where ε_{res}represents the residual strain associated with pre-existing curvature prior to strengthening (Stage III). Before TRC installation, $\varepsilon_{res} = 0$.

2.2.4 Constitutive relationships of materials

Concrete in compression is described using the parabolic–rectangular model proposed by Hognestad. The ascending branch is defined by

$$\sigma_c = f_c' \left[2\left(\frac{\varepsilon_c}{\varepsilon_{c0}}\right) - \left(\frac{\varepsilon_c}{\varepsilon_{c0}}\right)^2\right], \quad 0 \le \varepsilon_c \le \varepsilon_{c0} \tag{5}$$

where $f_c'$is the compressive strength, $\varepsilon_{c0}$is the strain at peak stress.

For $\varepsilon_{c0} < \varepsilon_c \le \varepsilon_{cu}$, the stress is taken as constant at f_c' until crushing.

Assuming a linear strain distribution, the compressive force is obtained by integration over the compression zone:

$$C_c = b\int_0^c \sigma_c\,(y)dy \tag{6}$$

Substituting the parabolic expression and integrating yields the closed-form expression:

$$C_c = bcf_c'\left(\frac{\varepsilon_c}{\varepsilon_{c0}} - \frac{\varepsilon_c^2}{3\varepsilon_{c0}^2}\right) \tag{7}$$

This expression is valid for $\varepsilon_c \le \varepsilon_{c0}$. For $\varepsilon_c > \varepsilon_{c0}$, the rectangular plateau contribution is included accordingly.

The centroid of the compressive stress block is given by

$$z_c = \frac{c(8\varepsilon_{c0} - 3\varepsilon_c)}{4(3\varepsilon_{c0} - \varepsilon_c)} \tag{8}$$

This formulation preserves nonlinear compression behaviour while maintaining an explicit sectional solution.

The longitudinal steel reinforcement is modeled using a bilinear elastic–perfectly plastic constitutive law (Figure 3-a). In the elastic range, the steel stress is defined as $\sigma_s = E_s\varepsilon_s$, where $E_s$denotes the elastic modulus of steel and $\varepsilon_s$is the steel strain. Yielding occurs when the strain reaches the yield strain $\varepsilon_y = f_y/E_s$, where $f_y$is the yield strength of steel. Beyond this point, the stress is assumed to remain constant at $\sigma_s = f_y$, and strain hardening is neglected. This simplified representation is consistent with conventional RC sectional analysis and provides a stable basis for equilibrium-based moment–curvature calculations. This formulation applies to both tensile and compression reinforcement, provided that compression buckling is prevented. In cracked stages, the effective tensile steel force includes the additional contribution from local tension stiffening around the reinforcement.

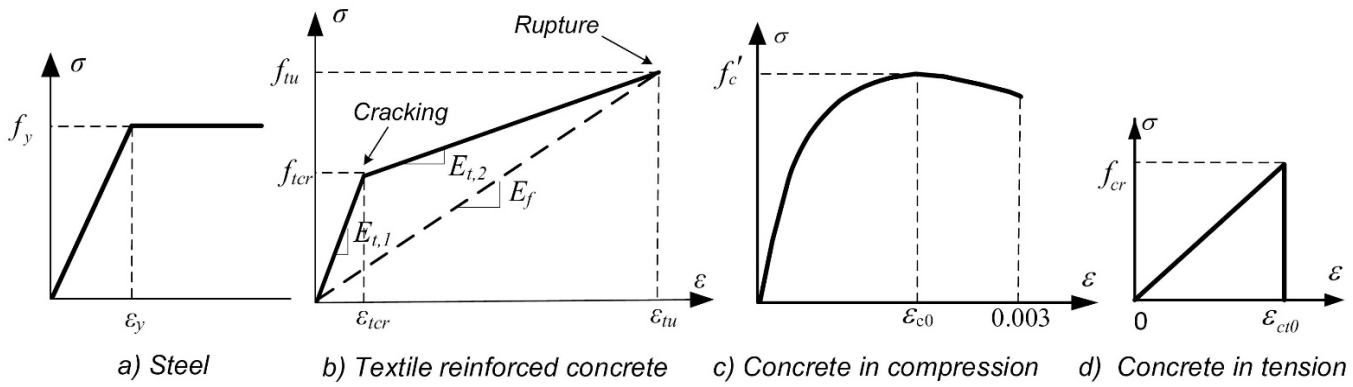

Figure 3 Constitutive stress–strain relationships of steel reinforcement, textile reinforcement, and concrete.

The TRC layer is modeled as a smeared composite material consisting of fine-grained concrete and embedded textile reinforcement. Perfect bond is assumed between textile and matrix, as well as at the interface between the TRC layer and the existing concrete, ensuring strain compatibility across the composite section. The tensile behavior of the TRC layer is represented by a bilinear stress–strain relationship reflecting matrix cracking and subsequent textile-dominated response (Figure 3-b).

Before matrix cracking, the tensile stress follows:

$$\sigma_t = E_{t,1}\varepsilon_t \quad \text{for} \quad \varepsilon_t \le \varepsilon_{t,cr} \tag{9}$$

where $E_{t,1}$is the effective elastic modulus of the composite layer and $\varepsilon_{t,cr}$corresponds to the cracking strain of the fine-grained matrix.

After matrix cracking, the tensile response becomes:

$$\sigma_t = f_{t,cr} + E_{t,2}\left(\varepsilon_t - \varepsilon_{t,cr}\right) \quad \text{for} \quad \varepsilon_{t,cr} < \varepsilon_t \le \varepsilon_{t,u} \tag{10}$$

where $E_{t,2}$represents the effective post-cracking stiffness governed by textile bridging and $\varepsilon_{t,u}$is the ultimate tensile strain of the TRC layer (Figure 3-c).

The corresponding tensile resultant is defined as:

$$T_{trc} = A_t\sigma_t \tag{11}$$

where $A_t$denotes the effective tensile area of the TRC layer. At ultimate, the tensile strain may be further limited by a debonding criterion.

2.2.5 General sectional equilibrium formulation

The flexural response of the TRC-strengthened RC beam is determined from strain compatibility and sectional force equilibrium. For a prescribed extreme concrete compressive strain ε_c, the neutral axis depth c is obtained from axial equilibrium under pure bending:

$$C_c + C_{s'} = T_s + T_c + T_{trc} \tag{12}$$

where $C_c$and $C_{s'}$denote the compressive forces in concrete and compression reinforcement, while T_s, T_c, and T_{trc}represent the tensile forces in steel, residual tensile concrete, and the TRC layer, respectively.

The strain distribution follows the plane-section assumption:

$$\varepsilon(y) = \phi(c - y) \tag{13}$$

Substitution of the constitutive relationships into Eq. (12) yields a quadratic equation in the unknown neutral axis depth,

$$\alpha_1 c^2 + \alpha_2 c + \alpha_3 = 0 \quad (14)$$

with coefficients depending on ε_c. Once c is determined, curvature is evaluated as

$$\phi = \frac{\varepsilon_c}{c} \quad (15)$$

The corresponding bending moment is obtained from moment equilibrium:

$$M = C_c z_c + C_{s'}(c - d') + T_s(d - c) + T_c z_{tc} + T_{trc}(d_{trc} - c) \quad (16)$$

where $z_c$denotes the lever arm of the concrete compressive resultant, $d$and $d'$are the effective depths of tensile and compression reinforcement, and $d_{trc}$is the centroidal depth of the TRC tensile force.

For cracked stages, the effective tensile steel force $T_{s,eff}$may replace T_s, while inactive components are omitted accordingly.

2.3 Stage-by-stage analytical solution

2.3.1 Stage I (0–1): Uncracked section (no TRC)

At low load levels, the concrete remains uncracked in tension. The strain distribution is linear over the entire section depth, and internal forces are resisted by concrete in both compression and tension together with elastic steel reinforcement. The sectional stiffness therefore corresponds to the gross (uncracked) section. The TRC layer is not yet activated, and its tensile force is zero ($T_{trc} = 0$).

For a prescribed extreme compressive strain ε_c, the neutral axis depth c is determined from axial equilibrium. Under the plane-section assumption, the curvature is evaluated as $\phi = \frac{\varepsilon_c}{c}$

Table 1 Forces components.

Concrete in compression	Compression steel	Tensile steel	Concrete in tension
$C_c = bcf_c^{'}\left(\frac{\varepsilon_c}{\varepsilon_{c0}} - \frac{1}{3}\left(\frac{\varepsilon_c}{\varepsilon_{c0}}\right)^2\right)$	$C_{s'} = E_s A_{s'} \frac{\varepsilon_c}{c}(c - d')$	$T_s = E_s A_s \frac{\varepsilon_c}{c}(d - c)$	$T_c = \frac{1}{2} E_c b \frac{\varepsilon_c}{c}(h - c)^2$

Substitution of the uncracked elastic force components (Table 1) into the general axial equilibrium equation leads to the quadratic form previously defined in Eq. (14).

$$bf_c'\left(\frac{\varepsilon_c}{\varepsilon_{c0}} - \frac{1}{3}\left(\frac{\varepsilon_c}{\varepsilon_{c0}}\right)^2\right)c^2 + E_s A_{s'}\varepsilon_c(c - d') - E_s A_s \varepsilon_c (d - c) - \frac{1}{2}E_c b \varepsilon_c (h - c)^2 = 0 \quad (17)$$

For Stage I, the corresponding coefficients are:

$$\alpha_1 = bf_c'\left(\frac{\varepsilon_c}{\varepsilon_{c0}} - \frac{1}{3}\left(\frac{\varepsilon_c}{\varepsilon_{c0}}\right)^2\right) - \frac{E_c b}{2}\varepsilon_c$$

$$\alpha_2 = E_s \varepsilon_c (A_s + A_s') + E_c b \varepsilon_c h$$

$$\alpha_3 = -\left[E_s \varepsilon_c (A_s d + A_s' d') + \frac{E_c b}{2}\varepsilon_c h^2\right] \quad (18)$$

Stage I terminates when the tensile stress in concrete reaches the cracking strength f_{cr}.

2.3.2 Stage II (1–2): Cracked RC section prior to strengthening

When the tensile stress at the extreme tension fibre reaches the concrete tensile strength f_{cr}, flexural cracking initiates and progressively propagates upward with increasing load. Although cracking develops, the tensile resistance of concrete is not completely eliminated. Two residual tensile mechanisms remain active: (i) local tension stiffening around

the tensile reinforcement due to bond interaction between steel and surrounding concrete, and (ii) the remaining effective tensile concrete between cracks below the neutral axis.

Tensile steel (with tension stiffening) is idealized as

$$T_s = E_s A_s \frac{\varepsilon_c}{c}(d-c) + \frac{1}{2} f_{cr} b(2a) \tag{19}$$

If cracking does not extend to the neutral axis ($h_{te} > c$), the remaining effective tensile concrete contributes

$$T_c = \frac{1}{2} E_c b \frac{\varepsilon_c}{c} h_{te}^2 \tag{20}$$

The TRC layer is not yet engaged ($T_{trc} = 0$). Substitution of the above force components into the general axial equilibrium equation and subsequent rearrangement lead to the quadratic expression in the neutral axis depth previously defined in Eq. (14). For Stage II (cracked section prior to strengthening), the corresponding coefficients are given as follows:

$$\alpha_1 = b f_c' \left(\frac{\varepsilon_c}{\varepsilon_{c0}} - \frac{1}{3} \left(\frac{\varepsilon_c}{\varepsilon_{c0}} \right)^2 \right)$$

$$\alpha_2 = E_s \varepsilon_c (A_s + A_{s'}) - \frac{1}{2} f_{cr} b(2a)$$

$$\alpha_3 = -\left[E_s \varepsilon_c (A_s d + A_{s'} d') + \frac{1}{2} E_c b \varepsilon_c h_{te}^2 \right] \tag{21}$$

2.3.3 Stage III (2–3): Partial Unloading Prior to Strengthening (No TRC)

Before installation of the TRC layer, the beam is partially unloaded from the service load level $P_{ser}$to a prescribed strengthening level P_{str}. Although the external bending moment decreases during unloading, the flexural cracks formed at $P_{ser}$are assumed to remain open and irreversible. No crack closure or stiffness recovery of the tensile concrete is considered.

As a consequence, the cracked section configuration established at $P_{ser}$is preserved during unloading. In particular, the effective tensile concrete region does not revert to the state corresponding to the loading path at the same load level P_{str}. The tensile stiffness of the section therefore remains reduced, even though the applied bending moment has decreased.

Due to irreversible crack opening and possible inelastic steel strains, the section does not recover its original elastic stiffness. A residual strain field and a residual curvature persist at P_{str}. Therefore, for an identical bending moment level, the curvature and deflection along the unloading path are larger than those obtained along the initial loading branch.

The unloading response is modeled by enforcing sectional equilibrium of the already cracked section under the reduced bending moment M_{str}, while retaining the same effective tensile mechanisms defined in Stage II (i.e., steel tension, bar-level tension stiffening, and remaining effective tensile concrete between cracks). The resulting curvature at P_{str}defines the initial geometric configuration at the time of TRC installation.

Subsequent strengthening analysis is then performed by superimposing curvature increments onto this residual state.

2.3.4 Stage IV (3–4): Strengthened section with uncracked TRC layer

After strengthening, the beam is reloaded from the residual state defined in Stage III. At this stage, the TRC layer remains uncracked and behaves elastically. Due to the pre-existing deformation, the TRC layer does not carry initial force at installation. Its contribution is therefore governed by strain increments relative to the strengthening state, rather than the total strain in the section.

The residual curvature at strengthening is treated as a constant:

$$\phi_{str} = \frac{\varepsilon_{c,str}}{c_{str}} \tag{22}$$

To explicitly account for the pre-existing deformation state at the time of strengthening, the tensile strain in the TRC layer is formulated in an incremental form with respect to the curvature at strengthening, as follows:

$$\varepsilon_{trc} = (\phi - \phi_{str})(d_{trc} - c) \tag{23}$$

Assuming linear elastic behavior before cracking, the corresponding tensile force in the TRC layer is

$$T_{trc} = E_{trc} A_{trc} (\phi - \phi_{str})(d_{trc} - x) \tag{24}$$

Substitution of the updated TRC tensile force into the general axial equilibrium equation yields the quadratic form with coefficients:

$$\alpha_1 = b f_c' \left(\frac{\varepsilon_c}{\varepsilon_{c0}} - \frac{1}{3} \left(\frac{\varepsilon_c}{\varepsilon_{c0}} \right)^2 \right) + E_t A_t (\phi - \phi_{str})$$

$$\alpha_2 = E_s \varepsilon_c (A_s + A_{s'}) - \tfrac{1}{2} f_{cr} b (2a) - E_t A_t (\phi - \phi_{str}) d_{trc}$$

$$\alpha_3 = -\left[E_s \varepsilon_c (A_s d + A_{s'} d') + \tfrac{1}{2} E_c b \varepsilon_c h_{te}^2 \right] \tag{25}$$

Stage IV terminates when the TRC tensile strain reaches the cracking strain $\varepsilon_{t,cr}$.

2.3.5 Stage V (4–5): Cracking of the TRC layer

When the tensile strain in the TRC layer exceeds the cracking strain $\varepsilon_{t,cr}$, matrix cracking develops in the fine-grained composite layer and the tensile response becomes governed by textile bridging. The TRC stress–strain relationship transitions to the second (post-cracking) branch. Although the sectional stiffness decreases relative to Stage IV, it remains higher than that of the unstrengthened cracked RC beam. Tension stiffening in the original RC substrate continues to operate.

Rearranging leads to the quadratic form with coefficients:

$$\alpha_1 = b f_c' \left(\frac{\varepsilon_c}{\varepsilon_{c0}} - \frac{1}{3} \left(\frac{\varepsilon_c}{\varepsilon_{c0}} \right)^2 \right) + E_t A_t (\phi - \phi_{str})$$

$$\alpha_2 = E_s \varepsilon_c (A_s + A_{s'}) - \tfrac{1}{2} f_{cr} b (2a) - E_t A_t (\phi - \phi_{str}) d_{trc}$$

$$\alpha_3 = -\left[E_s \varepsilon_c (A_s d + A_{s'} d') + \tfrac{1}{2} E_c b \varepsilon_c h_{te}^2 \right] \tag{26}$$

Stage V continues until a governing limit state (steel yielding, concrete crushing, or TRC debonding) is reached.

2.3.6 Stage VI (5–6): Post-yielding and ultimate response

At higher load levels, yielding of the tensile steel reinforcement may occur. Beyond yielding, additional moment capacity is primarily provided by curvature increase and the contribution of the TRC layer. The effective tensile steel force becomes

$$T_s = A_s f_y + 0.5 f_{cr} b (2a) \tag{27}$$

The effective tensile strain in the TRC layer may be limited by a debonding criterion, such that

$$\varepsilon_{t,eff} = min(\varepsilon_t, 0.0012) \tag{28}$$

Substitution into the general axial equilibrium equation yields with coefficients:

$$\alpha_1 = bf_c'\left(\frac{\varepsilon_{cu}}{\varepsilon_{c0}} - \frac{1}{3}\left(\frac{\varepsilon_{cu}}{\varepsilon_{c0}}\right)^2\right)$$

$$\alpha_2 = E_s A_{s'}\varepsilon_{cu} - A_s f_y - E_t A_t \varepsilon_t$$

$$\alpha_3 = -\left[E_s A_{s'}\varepsilon_{cu} d' + \frac{1}{2}E_c b \varepsilon_{cu} h_{te}^2\right] \quad (29)$$

The ultimate state is reached when any governing limit condition is satisfied:

$$\varepsilon_c = \varepsilon_{cu}, \quad \varepsilon_{t,eff} = \varepsilon_{t,u}, \quad \text{or} \quad \varepsilon_t \geq 0.0012 \quad (30)$$

The bending moment is evaluated using the general expression defined in Section 2.4.

2.4 Calculation of Mid-Span Deflection

The mid-span deflection of the beam is determined using the bending moment–curvature diagram and Xu's method (Xu et al. 2009). This approach simplifies the analysis by excluding certain factors, such as stiffness contributions from uncracked concrete between cracks and additional deflection from inclined cracks. Figure 4 depicts the deflection calculation method between two points, A and B. The deflection is calculated as:

$$\Delta_{A'B} = \int_B^A r d\theta = \int_A^B -r\frac{M(r)}{E(r)I(r)}dx = \int_A^B -r\phi(r)dx \quad (31)$$

With $d_\theta$is the angle of inclination of the element d_x; *x* and *r* are the distances from point A and point B to the element d_x.

For a simple beam subjected to 4-point bending, using 2 symmetrically placed concentrated loads, the rotation angle of point E in the middle of the span is 0 (= 0). Therefore, the deflection at point D affecting point E is shown as:

$$\Delta_D = \Delta_E - \int_D^E r\phi(r)dx \quad (32)$$

Since the deflection at the support D is zero ($\Delta_D = 0$), the deflection at point E is determined:

$$\Delta_E = \int_D^E r\phi(r)dx \quad (33)$$

This method provides an accurate calculation of mid-span deflection while relying on simplified assumptions for practical application.

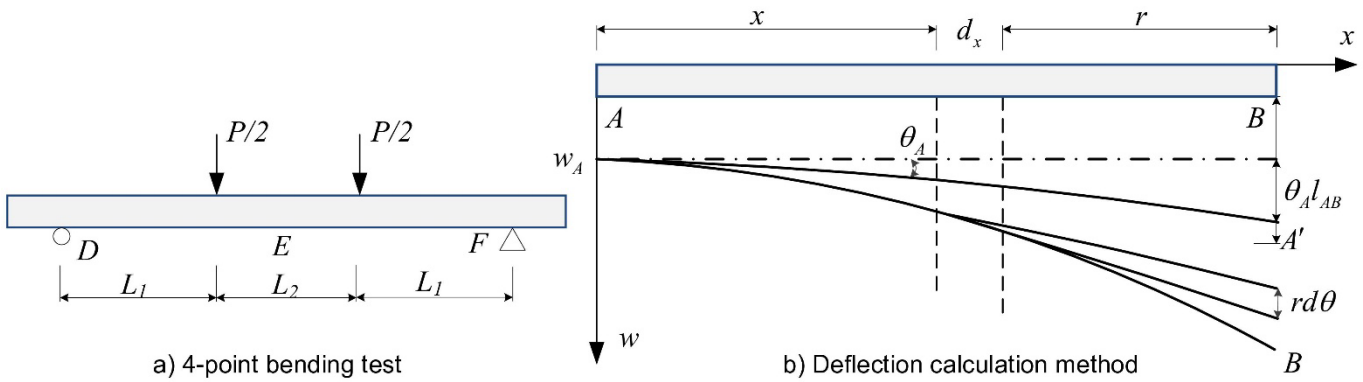

Figure 4. Method for determining beam deflection

3 EXPERIMENTAL VALIDATION

To assess the reliability of the proposed analytical model, an experimental program was conducted using full-scale RC beams extracted from the Ben Cho Bridge. Field-aged structures are influenced by long-term loading, environmental exposure, and material degradation; therefore, validation against real components is essential to confirm the model's practical applicability.

The test program aimed to (i) evaluate the residual flexural capacity of the aged RC beams and (ii) examine the effectiveness of TRC strengthening applied under realistic conditions. Measured responses—including load–deflection behavior, crack development, strain distribution, and failure mode—were compared with theoretical predictions.

3.1 Bridge Description and Test Specimens

The Ben Cho Bridge, constructed in 1995 in Ha Tinh Province, Vietnam, remained in service for approximately 30 years before being replaced in 2024. Over time, repeated overloading and environmental effects led to cracking and material deterioration, although severe chloride damage was not observed due to its inland location. The 4.5 m-wide deck consisted of five precast RC slab beams connected by wet joints and topped with a 50 mm in-situ concrete overlay, forming a composite deck system. Three central beams (rectangular shape with 1000 × 300 mm dimensions) and two edge beams (0.75 m wide, L-shaped) composed the superstructure. During dismantling, careful removal procedures were adopted to preserve the in-service condition of the beams. Two central beams were extracted and transported to the laboratory for detailed material characterization and flexural testing (Figure 5). The experimental results provide a reliable benchmark for validating the proposed analytical model under realistic conditions.

Figure 5 Aged condition of Ben Cho Bridge and retrieval of precast RC slab beams for full-scale experimental testing.

Prior to structural testing, material characterization was conducted to obtain reliable input parameters for the analytical model. Concrete cores (110 × 220 mm) were extracted from the beams. The average compressive strength was 22.4 MPa, slightly lower than the original design value, reflecting long-term service effects such as environmental exposure and repeated loading.

The reinforcement layout consisted of twelve Ø18 mm bars in the tension zone, four Ø12 mm bars in compression, and Ø6 mm stirrups spaced at 300 mm. Tensile tests on extracted steel samples indicated an average yield strength of 352.3 MPa, an ultimate strength of 554.8 MPa, and an elastic modulus of 198.3 GPa. Although the yield plateau was not clearly defined, the steel maintained adequate ductility and strength. These measured properties were directly incorporated into the analytical model.

3.2 Test Setup and Loading Configuration

Full-scale four-point bending tests were performed to evaluate flexural behavior. The beams had a 6.1 m span, with 2.3 m shear spans and a 1.5 m constant-moment region at mid-span (Figure 6). This configuration provided a nearly uniform bending zone with minimal shear influence, facilitating comparison with theoretical predictions.

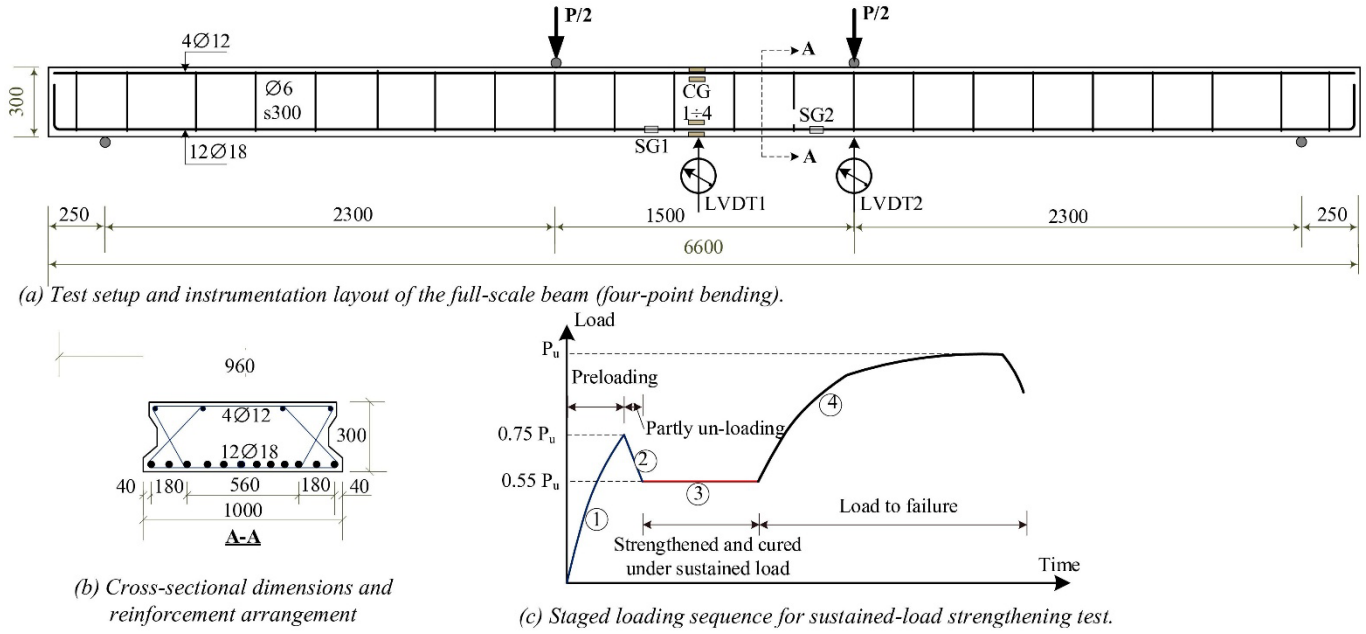

(a) Test setup and instrumentation layout of the full-scale beam (four-point bending).

(b) Cross-sectional dimensions and reinforcement arrangement

(c) Staged loading sequence for sustained-load strengthening test.

Figure 6 Experimental configuration of the full-scale beam

Loading was applied through two 1000 kN hydraulic jacks mounted on a rigid reaction frame (Figure 7). After a small pre-load (5 kN) to ensure proper seating, the load was increased incrementally (≈1 kN per step) until failure. Instrumentation included load cells, pressure gauges, and two LVDTs at mid-span for deflection measurements. Strain gauges were installed on longitudinal reinforcement and along the beam depth to capture strain distribution. Crack development was monitored using a crack-width gauge. This setup enabled detailed recording of load–deflection response, crack evolution, stiffness degradation, and ultimate failure behavior.

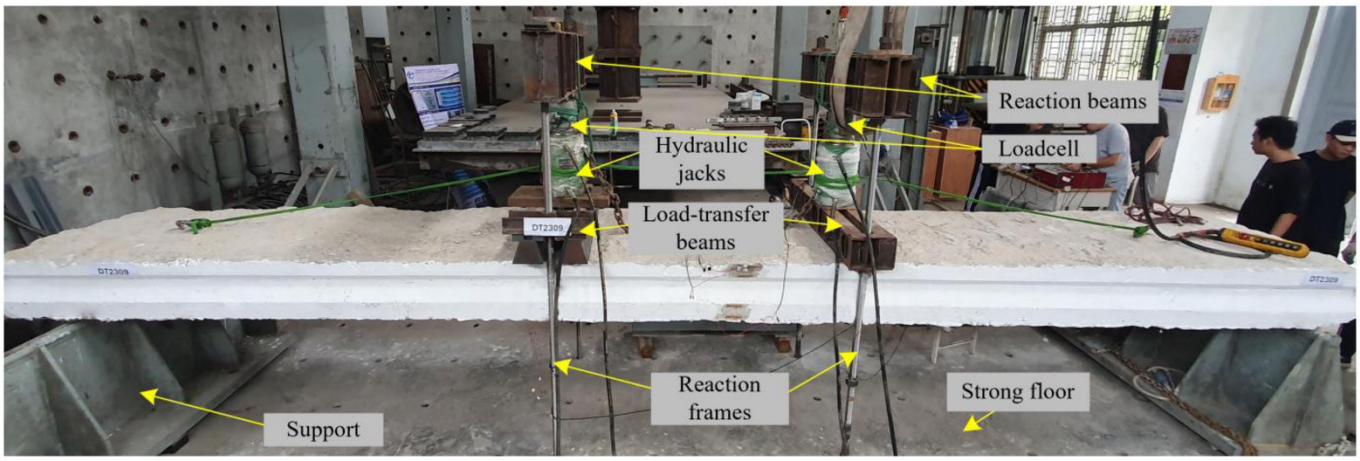

Figure 7 Experimental Setup Configuration.

3.3 Behavior of the Control Specimen and Preloaded Specimen

3.3.1 Control Specimen BC1

The unstrengthened beam (BC1) was tested first to establish a baseline flexural response for subsequent comparison and analytical model validation. The load–deflection curve remained linear up to approximately 60 kN (excluding the beam self-weight of about 50 kN), indicating uncracked elastic behavior governed by the gross sectional stiffness (Figure 8). At this load level, the first visible flexural cracks appeared within the constant moment region.

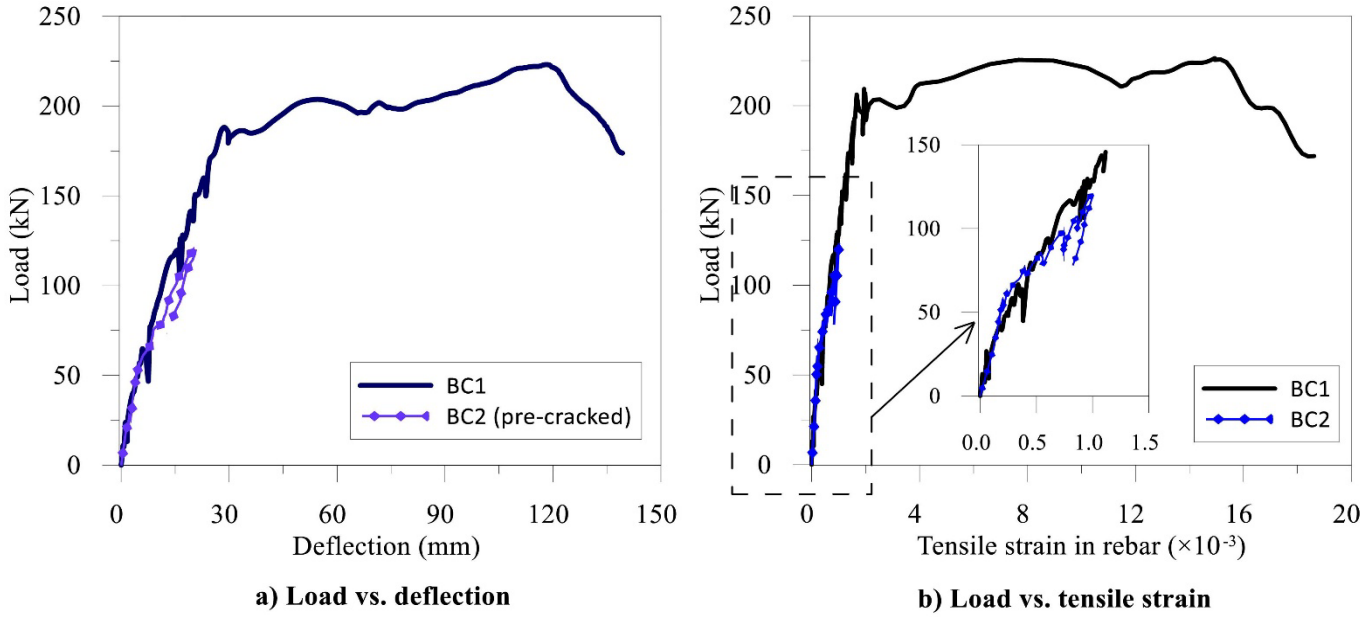

Figure 8 Load vs. deflection and tensile strain relationships of BC1 and pre-cracked BC2

Beyond crack initiation, the stiffness decreased markedly as tensile stresses were progressively transferred from the concrete to the longitudinal reinforcement. With increasing load, crack propagation and widening led to gradual stiffness degradation. At approximately 190–200 kN, the tensile reinforcement approached the yielding threshold, accompanied by crack widths reaching about 0.5 mm at mid-span (Figure 9).

Figure 9 Failure mode and crack pattern structure of BC1 beam

The beam ultimately failed at a load of 226 kN, corresponding to mid-span deflections of approximately 120–140 mm. Failure was governed by concrete crushing in the compression zone following significant plastic deformation of the tensile reinforcement, with measured steel strains exceeding 16‰. The overall response followed the classical three-stage behavior—uncracked elastic, cracked elastic, and post-yield—providing a reliable reference for evaluating the performance of the strengthened specimen and for comparison with analytical predictions.

3.3.2 Preloaded Specimen Prior to Strengthening (BC2)

To simulate in-service damage conditions prior to strengthening, the second beam (BC2) was subjected to a controlled preloading procedure designed to induce stable flexural cracking while preserving the structural integrity of the member. The beam was gradually loaded to 125 kN, corresponding to approximately 55–60% of the ultimate capacity of BC1. This load level exceeded the cracking moment but remained below the yielding threshold of the longitudinal reinforcement.

The load–deflection response during preloading closely followed that of BC1 in the elastic and early cracked regimes (Figure 8), indicating comparable initial stiffness and material properties between the two specimens. First visible flexural cracks appeared at approximately 60–65 kN within the constant moment region, consistent with the behavior observed in BC1.

Strain measurements confirmed that the tensile reinforcement remained within the elastic range during preloading, with maximum recorded strains not exceeding approximately 1.7‰. The compressive strain in concrete remained limited

to about 0.6–0.85‰, well below the ultimate crushing strain. These results indicate that the beam was brought to a controlled cracked state without inducing steel yielding or severe damage.

After reaching the target preload, the beam was partially unloaded and maintained at a sustained load of 80 kN during TRC application and the subsequent 28-day curing period. This sustained load level was selected to represent a realistic service condition during strengthening, assuming partial reduction of live load. Importantly, unloading did not restore the original stiffness, and residual deflection and tensile strain were observed, confirming the irreversibility of cracking and the presence of a non-zero initial strain state prior to strengthening.

Figure 10 Crack pattern of BC2 during preloading and sustained loading

The resulting crack pattern, shown in Figure 10, consisted of distributed flexural cracks concentrated within the constant moment region. Crack spacing ranged from approximately 90 to 150 mm, with maximum crack widths between 0.15 and 0.25 mm under sustained loading. The cracks were stable and uniformly distributed, with no evidence of crack localization or progressive damage. Only a limited number of minor flexural–shear cracks were observed near the loading points, and no shear-dominated failure mechanisms were activated.

This pre-cracked condition corresponds to a controlled service-level damage state, characterized by distributed cracking, non-yielded reinforcement, and residual deformation. From a mechanical perspective, this state is particularly significant, as the presence of residual curvature and reduced effective stiffness directly influences the subsequent stress redistribution, tension stiffening behavior, and stiffness recovery after TRC strengthening. Therefore, BC1 represents the intact reference condition, while BC2 provides a realistic representation of an aged and cracked member under sustained service load, forming a sufficiently reliable basis for comparative assessment of the strengthening effectiveness under realistic conditions.

It should be noted that both BC1 and BC2 were extracted from the same bridge and share identical geometry, reinforcement configuration, and construction conditions. Material characterization, including concrete compressive strength and reinforcement properties, indicated comparable mechanical properties between the two specimens. Furthermore, the similar load–deflection and strain responses observed during the initial loading stage (Figure 8) confirm the consistency of their structural behavior prior to strengthening.

3.4 TRC-Strengthened Beam

The strengthening system comprised three layers of carbon textile embedded in a fine-grained cementitious mortar, forming an approximately 20 mm-thick TRC layer bonded to the tension face of the beam. Prior to application, the concrete surface was mechanically roughened and thoroughly cleaned to enhance bond performance and ensure effective stress transfer. A thin bonding layer was first applied, after which the textile meshes were sequentially pressed into alternating layers of fine-grained mortar approximately 5 mm thick, ensuring proper impregnation and composite interaction (Figure 11). The beam was maintained under a sustained load of 80 kN throughout installation and the 28-day curing period, allowing the TRC layer to harden and develop composite action under realistic in-service stress conditions.

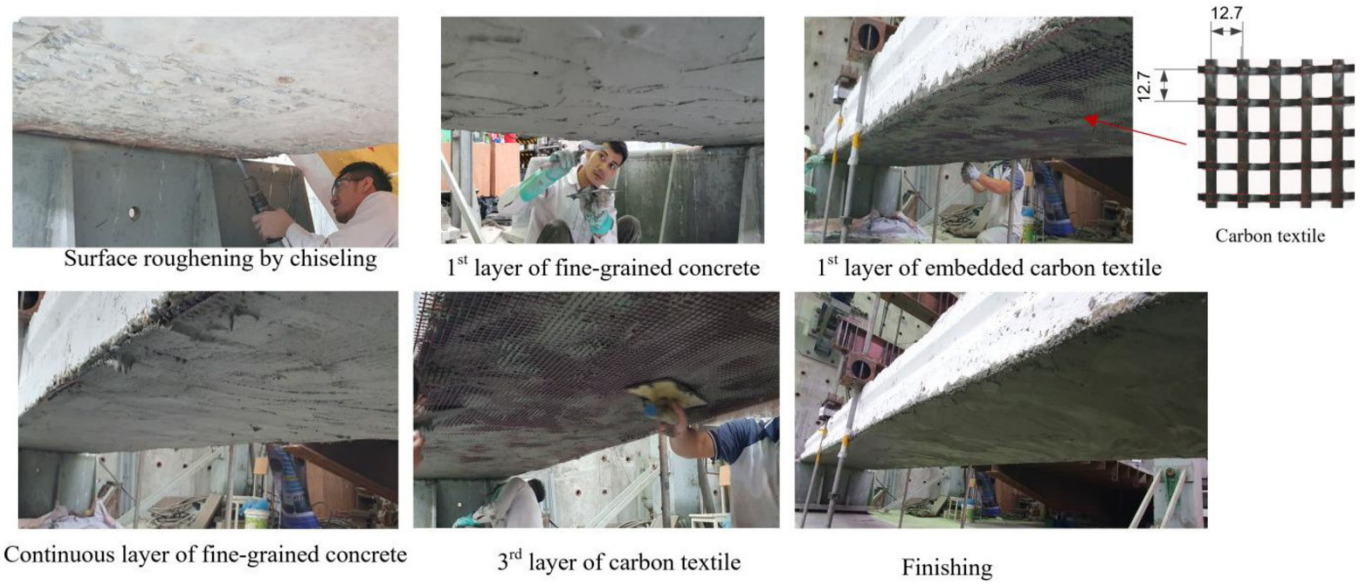

Figure 11 Strengthening process

After 28 days of curing under the sustained load of 80 kN, beam BC2 was reloaded to failure using the same four-point bending configuration as BC1. The comparison between the two beams highlights the mechanical contribution of the TRC layer in terms of stiffness recovery, strain redistribution, and ultimate capacity enhancement.

From the load–deflection response, BC2 initially follows the residual deformation path corresponding to the sustained 80 kN preload. Beyond this level, the slope of the load–deflection curve becomes steeper than that of BC1 in the corresponding cracked stage (Figure 12-a). Between approximately 80 kN and 180 kN, BC2 exhibits noticeably higher flexural stiffness, with smaller incremental deflections for the same load increase. For instance, at a load level near 200 kN, BC1 shows mid-span deflections on the order of 90–100 mm, whereas BC2 remains below approximately 70–80 mm. This stiffness recovery indicates effective crack-bridging by the TRC layer and partial restoration of sectional rigidity through composite action between textile, fine-grained matrix, and cracked substrate concrete.

The load–tensile strain curves further confirm this behavior (Figure 12-b). In BC1, steel yielding begins around 190–200 kN, corresponding to tensile strains approaching the yield threshold (≈2.0–2.2‰ depending on measured data). In contrast, BC2 reaches comparable steel strain levels at significantly higher loads. The yielding point in BC2 shifts upward, occurring closer to 230–240 kN. This delay demonstrates that part of the tensile force is transferred to the TRC layer, reducing demand on the internal steel reinforcement and postponing yielding.

Crack development also differs substantially. In BC2, cracks remain narrower and more uniformly distributed throughout loading. While BC1 exhibited crack widths approaching 0.5 mm near yielding, BC2 maintained visibly smaller crack openings over a broader load range. The more uniform crack pattern reflects improved tension stiffening and stress redistribution provided by the textile reinforcement embedded in the cementitious matrix.

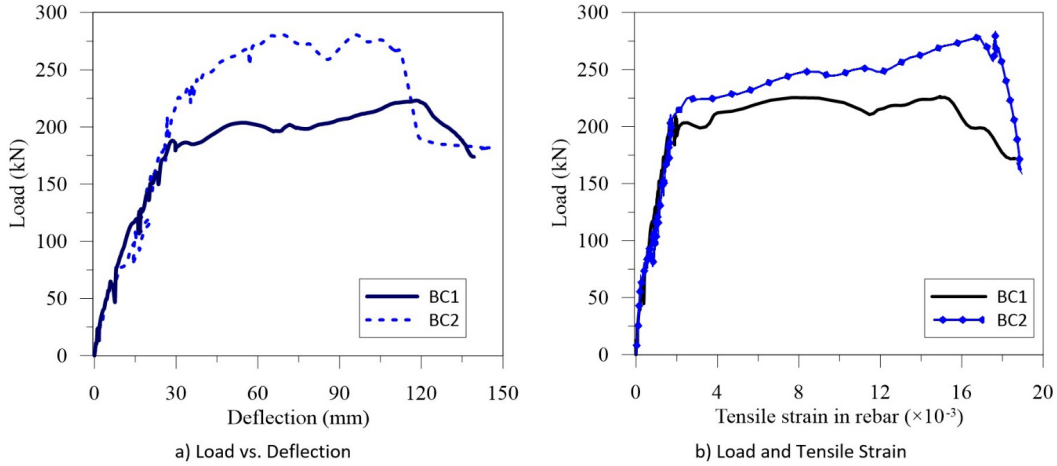

Figure 12 Comparison between control beam and strengthened beam

The ultimate load of BC2 reached approximately 282 kN, compared to 226 kN for BC1, representing an increase of roughly 25%. This enhancement is consistent with the additional tensile capacity provided by the TRC layer and confirms that the strengthening system was structurally engaged beyond the service range. At failure, BC2 exhibited larger steel strains (approaching 18–19‰) and higher curvature prior to collapse, indicating improved ductility.

Failure mode remained flexural in nature. Concrete crushing in the compression zone governed ultimate failure, similar to BC1. However, crack propagation in BC2 was better controlled, and partial TRC debonding was observed only near ultimate load, after compression failure had initiated (Figure 13). This sequence suggests that the textile reinforcement was effectively utilized throughout the loading process and that bond performance was sufficient to mobilize its tensile capacity before debonding occurred.

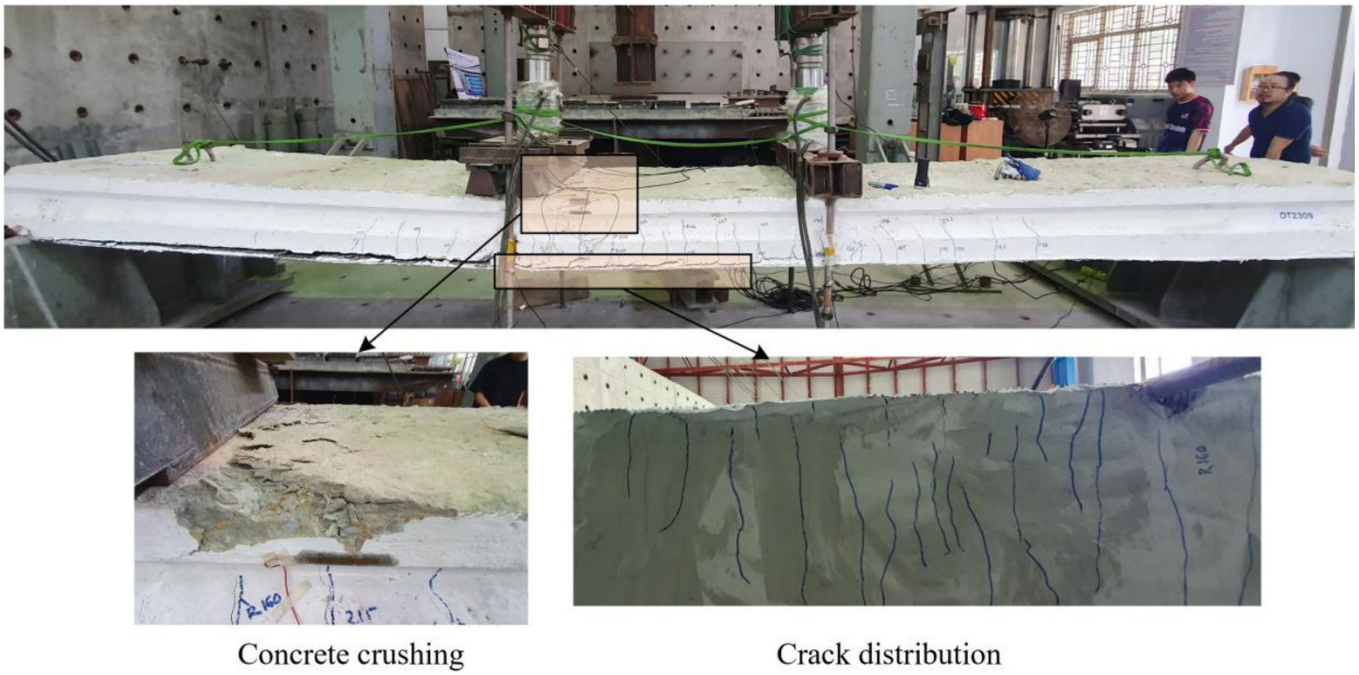

Figure 13 Failure mode and crack pattern

3.5 Comparison with Theoretical Predictions and Model Validation

Figure 14 presents the calculated load–deflection responses of specimens BC-1 and BC-2, including the contribution of self-weight. The curves were obtained using the stage-wise sectional model developed in Section 2, implemented within a Python-based computational framework to evaluate curvature, internal force equilibrium, and stiffness evolution throughout the loading process. As shown in Figure 14, both beams exhibit the characteristic multi-stage behavior predicted by the proposed model. The initial linear segment corresponds to the uncracked stiffness of the gross section. Following cracking, a distinct reduction in stiffness is observed, reflecting the transition to the tension-stiffening regime of the cracked concrete. For the unstrengthened beam (BC1), the post-cracking response gradually approaches a simplified bilinear behavior, as the tensile contribution of cracked concrete diminishes and the response becomes dominated by steel reinforcement.

After strengthening, specimen BC-2 shows a steeper post-cracking slope compared to BC-1, indicating the additional tensile contribution of the TRC layer. This stiffness enhancement is consistently captured by the analytical model, which also reproduces the subsequent nonlinear response associated with progressive activation of the textile reinforcement and yielding of the internal steel reinforcement. In contrast to BC1, the strengthened beam exhibits a nonlinear response due to the continued tensile contribution of the TRC layer after steel yielding, including tension stiffening and progressive load redistribution. At higher load levels, both analytical and experimental results indicate that the ultimate state is governed by crushing of the concrete in compression. Failure occurs when the extreme compressive strain reaches the adopted limit of $\varepsilon_c = 0.003$. At this stage, the textile reinforcement has not reached its debonding or rupture strain, confirming that the failure mode is compression-controlled rather than TRC-controlled.

It should be noted that this assumption introduces a limitation in the present formulation, as post-peak softening of concrete and alternative failure mechanisms, such as TRC debonding or progressive crushing, are not explicitly modeled. Nonetheless, the overall agreement between the Python-based predictions and the experimental results

demonstrates that the proposed analytical approach provides an accurate and mechanically consistent representation of the flexural response of TRC-strengthened RC beams under realistic conditions.

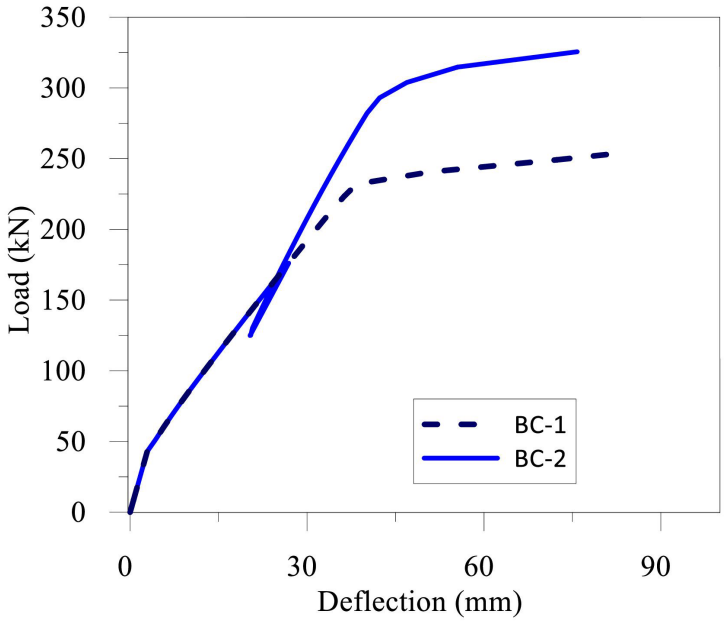

Figure 14 Calculated load–deflection relationships of beams BC-1 and BC-2, including the effect of self-weight.

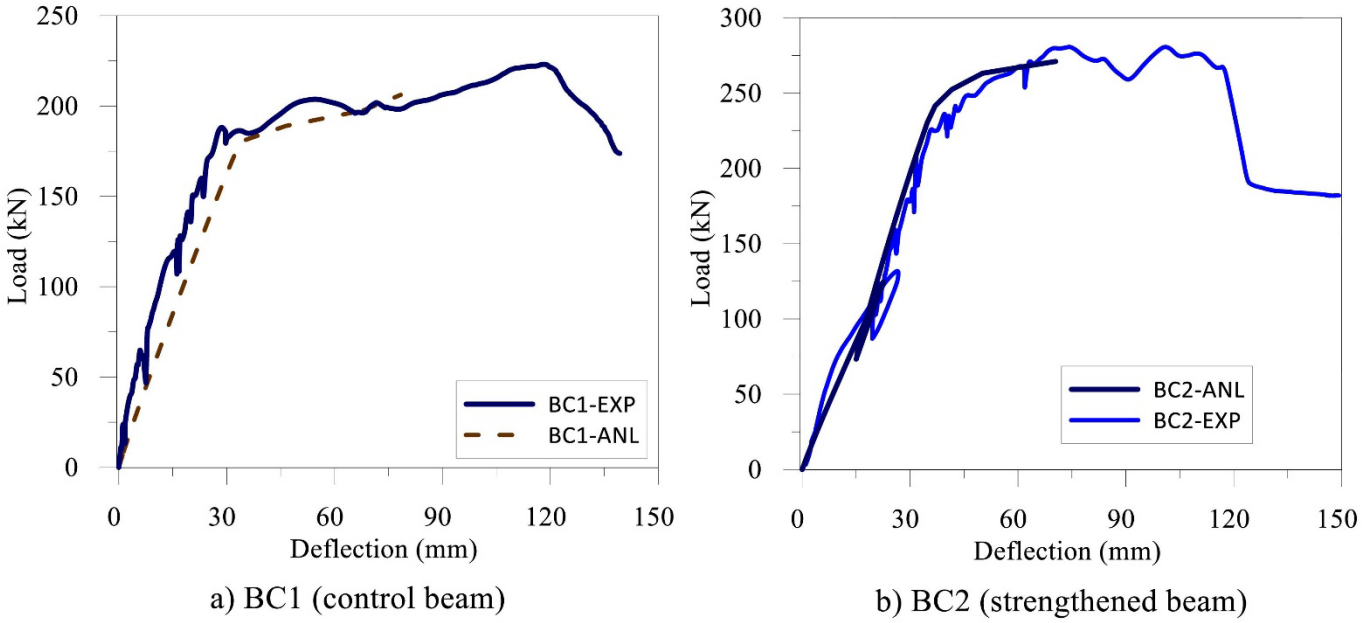

Figure 15 Experimental and analytical load–deflection curves of BC1 and BC2

Figure 15 compares the analytical (ANL) and experimental (EXP) load–deflection responses after correcting the analytical curves by subtracting 50 kN to remove the self-weight contribution included in the model. This correction allows a consistent comparison with the experimental measurements, where self-weight is inherently included in the recorded response. Overall, the proposed formulation reproduces the governing trends for both the control beam (BC1) and the TRC-strengthened beam (BC2), with particularly good agreement in the pre-peak range. For BC1, the analytical curve captures the transition from the initial quasi-linear branch to the cracked stiffness regime, although it is slightly more compliant during early loading. At a deflection of 30 mm, EXP reaches approximately 180–190 kN, whereas ANL predicts about 165–175 kN (≈5–10% lower). In the mid-range (50–80 mm), deviations remain within ±5%. The ultimate state is governed by crushing of the concrete in compression, consistent with the strain limit adopted in the model. For BC2, agreement is closer, with differences generally below 5% up to 70–80 mm. The strengthened beam also failed in a compression-controlled mode, with concrete crushing occurring before textile rupture or debonding. The textile

reinforcement did not reach its rupture or effective debonding strain, indicating reserve tensile capacity in the TRC layer. This behavior highlights a limitation of the present model, which is restricted to a concrete compressive strain of 0.003 and does not explicitly simulate post-peak softening or progressive debonding. Future research should incorporate advanced compression softening and bond–slip modeling to better capture post-peak behavior and alternative failure modes.

4 COMPARISON WITH DESIGN GUIDELINES

This section presents the analytical determination of flexural strengths for TRC-strengthened beams based on three design guidelines: ACI 549.4R-20 ,Zulassung Z-31.10-182, and CNR-DT 215/2018. In addition, the predictions from these guidelines are directly compared with those obtained from the proposed analytical model and the experimental results, to provide a consistent and comprehensive evaluation. While these guidelines adopt similar underlying assumptions and failure mechanisms to estimate ultimate flexural capacity, they differ notably in the tensile strain limits imposed on the textile reinforcement and the ultimate compressive strain considered for the concrete. In each case, it is assumed that plane sections remain plane and that the TRC layer is fully bonded to the concrete substrate (Figure 16). The maximum usable compressive strain of the concrete is typically taken as 0.003 in ACI-based approaches or 0.0035 according to Eurocode 2, and the textile reinforcement is treated as exhibiting linear-elastic behavior until failure. In addition to defining these material and sectional behaviors, potential failure modes must be carefully examined to ensure the reliability and safety of the strengthening solution. Such failure modes include concrete crushing in compression, yielding of internal steel reinforcement followed by concrete crushing, debonding of the TRC layer from the substrate, and tensile rupture of the textile reinforcement. By considering these potential failure scenarios, a more robust and accurate estimation of the ultimate flexural capacity of TRC-strengthened members can be achieved.

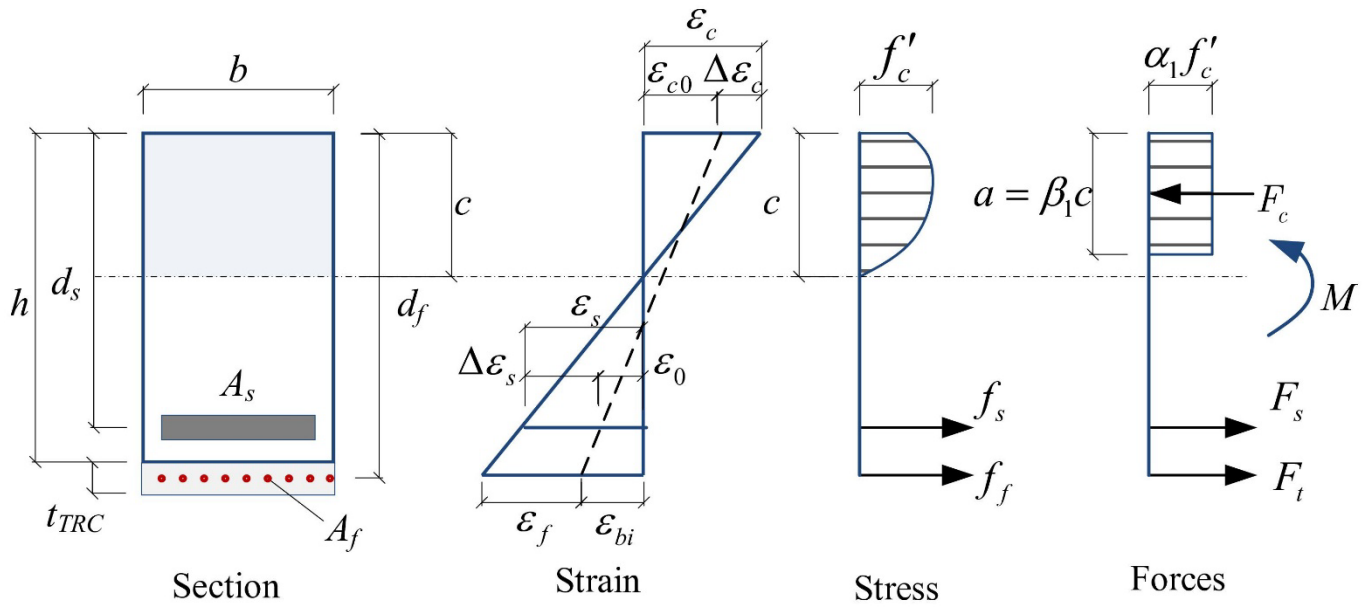

Figure 16. Representative strain and stress distributions within a TRC-strengthened concrete section

To determine the TRC's contribution, the effective tensile strain at ultimate (ε_{fd}) is identified and is subsequently multiplied by the elastic modulus of the textile (E_f) to obtain the tensile stress (f_{fd}). Once the strains and stresses have been established, the nominal flexural strength (M_n) is computed by integrating the contributions of both steel and TRC reinforcements.

$$M_n = A_s\varepsilon_s E_s\left(d_s - \frac{a}{2}\right) + A_f\varepsilon_f E_f\left(d_f - \frac{a}{2}\right) \tag{34}$$

A primary distinction among these design standards lies in the specified design tensile strain limits for the textile reinforcement at the ultimate limit state and the adopted ultimate compressive strain of the concrete.

According to ACI 549.4R-20, the effective tensile strain in the textile reinforcement (ε_{fe}) is limited to $\varepsilon_{fd} = \varepsilon_{fu} = 0.012$, while the ultimate compressive strain of the concrete is taken as $\varepsilon_{cu} = 0.003$.

Under CNR-DT 215/2018, the critical tensile strain in the textile reinforcement $\varepsilon_{f,d} = min\left(\varepsilon_{lim,\,comv,d}^{(\alpha)}, \varepsilon_{uf,d}\right)$depends on both the charactistic ultimate tensile strain ($\varepsilon_{uf,d}$) of the chosen strengthening system and the debonding-related critical strain ($\varepsilon_{lim,\,comv,d}^{(\alpha)}$). The value of $\varepsilon_{lim,\,comv,d}^{(\alpha)}$ was used to limit the textile's strain to avoid premature failure due to debonding at the interface. This strain is typically lower than the ultimate tensile strain and depends on the bond strength between the TRC layer and the concrete substrate. For the concrete, the ultimate compressive strain specified by CNR-DT 215/2018 is $\varepsilon_{cu} = 0.0035$

Under Z-31.10-182, the effective tensile strain in the textile reinforcement (ε_{fe}) is limited to $\varepsilon_{u,tex} = 0.0075$ and the ultimate compressive strain of the concrete is also taken as $\varepsilon_{cu} = 0.0035$.

Furthermore, CNR-DT 215/2018 and Z-31.10-182 offer more comprehensive guidance on the calculation of flexural capacity corresponding to a variety of potential failure modes. These guidelines also account for the influence of pre-existing and ongoing loads on the structure, as well as their effects on steel reinforcement strains prior to the implementation of strengthening measures. Table 2 summarizes the calculated flexural capacities of the strengthened beam according to the three design guidelines, allowing a direct comparison of their predictions with respect to the experimental results.

Table 2 Computed flexural capacities of the strengthened beam according to three design guidelines.

Factor	Symbol	Unit	ACI 549.4R-20	CNR-DT 215/2018	Z-31.10-182
Section width	b	mm	1000	1000	1000
Section depth	h	mm	300	300	300
Concrete compressive strength	f_{cm}	MPa	22.4	22.4	22.4
Steel yield strength	f_y	MPa	352.3	352.3	352.3
Textile tensile rupture strength	f_{fu}	MPa	2700	2700	2700
Steel modulus of elasticity	E_s	MPa	198000	198000	198000
Textile modulus of elasticity	E_f	MPa	185000	185000	185000
Effective steel depth	d_s	mm	260	260	260
Effective textile depth	d_f	mm	315	315	315
Initial steel strain due to pre-existing loads	ε_{s0}	-	-	0.000234	0.0024
Code-defined ultimate concrete strain	ε_{cu}	-	0.003	0.0035	0.0035
Code-defined design textile strain	ε_{fu}	-	0.012	0.0086	0.0075
Effective textile strain	ε_{fe}	-	0.00735	0.00753	0.0075
Effective steel strain	ε_s	-	0.0018	0.0018	0.0018
Neutral axis depth	c	mm	91.29	97.85	97.91
Failure mode	-	-		Crushing of concrete	
Theoretical flexural capacity (moment)	*Theory*	kN.m	396.9	405.8	381.5
Dead load moment (self-weight)	*DL*	kN.m	33.14	33.14	33.14
Experimental applied moment (jack load)	*EXP*	kN.m	324.3	324.3	324.3
Ratio (EXP+DL)/Theory	*(EXP+DL)/Theory*	-	0.9	0.88	0.94

From the computed results, noticeable differences emerge among the three examined design approaches, while the proposed analytical model shows closer agreement with the experimental response. The predictions obtained using Z-31.10-182 align most closely with the experimental results, producing a test-to-theory ratio of 0.94. This indicates that the Z-31.10-182 approach provides a conservative and reasonably accurate estimate of the actual flexural capacity. In contrast, the predictions derived from ACI 549.4R-20 and CNR-DT 215/2018 are less accurate, with test-to-theory ratios of 0.9 and 0.88, respectively. For comparison, the proposed analytical model shows very close agreement with the experimental results, with deviations generally within approximately 5%, which is smaller than those obtained from the design guidelines. This improved accuracy can be attributed to the explicit consideration of sustained loading effects, residual strain, and the composite tensile behavior of the TRC system in the proposed formulation.

These results show that the experimental flexural capacity is approximately 10–12% lower than the theoretical predictions from ACI 549.4R-20 and CNR-DT 215/2018. The discrepancies can be attributed to differences in the defined ultimate strains, the influence of pre-existing steel strain, and assumptions related to failure modes. A notable concern arises from the fact that the calculated flexural capacities using these guidelines exceed the experimentally observed

values by approximately 6–12%. This overestimation could pose risks when strengthening structures under sustained loading, as it may fail to account for the pre-existing damage and long-term effects on structural behavior. Therefore, for in-service structures, careful consideration should be given to these discrepancies to ensure the reliability and safety of the strengthening design. In contrast, the proposed model provides a more consistent representation of the structural response under realistic service conditions, supporting its applicability for practical assessment of strengthened members.

5 RESULTS AND DISCUSSION

5.1 Global structural response and role of strengthening

The comparison between the control specimen (BC1) and the strengthened specimen (BC2) clearly demonstrates the effectiveness of TRC strengthening in enhancing flexural performance. Both beams exhibit the typical transition from uncracked to cracked behavior. However, BC2 shows a clearly improved response after cracking. It exhibits higher stiffness and a more gradual stiffness degradation. This behavior reflects the active role of the TRC layer in bridging cracks and redistributing tensile stresses across the section.

For the control beam, the response follows conventional reinforced concrete behavior. After cracking, tensile resistance is progressively transferred to the steel reinforcement, leading to a pronounced stiffness reduction. Once the steel yields, the response approaches a simplified bilinear form, as the contribution of cracked concrete in tension becomes negligible. In contrast, the strengthened beam exhibits a different load-carrying mechanism. The TRC layer continues to carry tensile stresses even after steel yielding. This results in a smoother stiffness transition and a nonlinear load–deflection response. As a result, stiffness degradation is delayed and deformation capacity is improved.

5.2 Influence of pre-damage and sustained loading

The pre-damaged condition of BC2 plays a critical role in its structural response. It provides a realistic representation of in-service bridge members. Unlike laboratory specimens, which are typically tested in an undamaged state, the beam in this study was pre-cracked and subjected to sustained loading prior to strengthening. This resulted in residual strains, reduced initial stiffness, and a non-zero curvature at the onset of strengthening.

The sustained load applied during strengthening is particularly significant, as it induces an initial strain state in the TRC system. Consequently, the textile reinforcement is activated under a pre-existing stress condition rather than from an unloaded state. This alters the stress redistribution mechanism and enhances the interaction between concrete, steel, and the TRC layer. Such behavior is representative of real strengthening scenarios, where complete unloading is rarely feasible.

These findings highlight the limitations of conventional design approaches, which generally assume idealized initial conditions and neglect residual stress–strain states. The results emphasize the importance of incorporating pre-damage and sustained loading effects to achieve a realistic assessment of strengthened members, especially for aging bridge structures.

5.3 Model performance and comparison with design approaches

The proposed analytical model shows very good agreement with the experimental results, with deviations generally within approximately 5%. The model accurately captures the key features of the structural response. These include stiffness transition after cracking, yielding of steel reinforcement, and the nonlinear response induced by the TRC layer.

For the control beam, the model reproduces the bilinear response associated with the transition from elastic to cracked stiffness and the dominance of steel reinforcement in the post-yield stage. For the strengthened beam, the model captures the nonlinear response arising from tension stiffening and the continued tensile contribution of the TRC layer. This demonstrates the capability of the formulation to represent the complex interaction between materials across different loading stages.

In contrast, existing design guidelines tend to overestimate the flexural capacity. This is mainly due to simplified assumptions, including the neglect of residual strains, sustained loading effects, and composite interaction mechanisms. As a result, code-based predictions may not fully reflect the actual behavior of strengthened members under realistic conditions.

5.4 Engineering implications

From an engineering perspective, the results clearly demonstrate that TRC strengthening is effective for in-service bridge members. This is particularly important for structures with pre-existing damage and sustained loading conditions. The improved stiffness, enhanced crack control, and increased deformation capacity observed in BC2 suggest that TRC systems can significantly extend the service life of aging infrastructure.

However, the comparison with design guidelines also indicates that caution is required when applying code-based predictions to real structures. The observed overestimation of flexural capacity highlights the need to account for the interaction between damage, sustained loading, and composite action. This is especially critical for long-span bridge members subjected to long-term service conditions.

Overall, the findings support the use of advanced analytical models that incorporate realistic boundary conditions and material interactions. By bridging the gap between laboratory assumptions and field conditions, the proposed model provides a more reliable basis for assessing and designing strengthened structures.

6 CONCLUSION

This study developed and experimentally validated a closed-form, stage-wise sectional analytical model for RC beams strengthened with carbon textile-reinforced concrete (TRC) under sustained service loading. This formulation provides a consistent mechanical framework for analyzing strengthened members under realistic in-service conditions.

The TRC layer is modeled as a composite material with bilinear tensile behavior, accounting for matrix cracking, textile bridging, and post-cracking stiffness evolution. In addition, tension stiffening of the original RC substrate and residual tensile concrete between cracks are consistently included, enabling a unified description of the multi-stage flexural response.

Experimental results from full-scale bridge slab beams after approximately 30 years of service demonstrate a clear enhancement in structural performance. The strengthened specimen exhibited an increase in ultimate load of approximately 25% compared to the control beam, together with significantly improved crack control, with crack widths and spacing reduced to approximately one-third to one-half of those in the unstrengthened beam.

Strain measurements confirm effective stress redistribution, with steel reinforcement reaching strains of approximately 16‰, while the carbon textile exhibited high strain utilization, in some regions exceeding the design limit suggested by ACI 549.4R-20.

The analytical predictions show good agreement with the experimental results. The discrepancies are generally within approximately 5% for the strengthened specimen and within about 10% for the control specimen in the pre-peak range. Compared with existing design approaches, the proposed model provides a more accurate representation of stiffness transition and residual-state behavior under sustained loading.

Among the examined design approaches, Z-31.10-182 provided the closest prediction to the experimental capacity, whereas ACI 549.4R-20 and CNR-DT 215/2018 overestimated the flexural strength by about 6–12%. This indicates that current code-based methods may be unconservative for pre-cracked, in-service members strengthened under sustained loading, since residual strain and staged activation effects are not explicitly considered.

Failure was governed by concrete crushing at $\varepsilon_c = 0.003$, indicating a compression-controlled mechanism with remaining tensile reserve in the TRC layer. The model does not explicitly account for post-peak softening or bond-related effects, which should be addressed in future studies.

Acknowledgments

The research is funded by the Vietnamese Ministry of Education and Training under grant number B2026-GHA-02.

Author's contributions: Conceptualization, H.C. Nguyen and T.T.M. Bui; Methodology, H.C. Nguyen; Investigation, H.C. Nguyen, D.D. Le and V.H. Vu; Data curation, D.D. Le and V.H. Vu; Formal analysis, H.C. Nguyen and C.H. Nguyen; Writing – original draft, H.C. Nguyen, D.D. Le and V.H. Vu; Writing – review & editing, H.C. Nguyen and T.T.M. Bui; Supervision, T.T.M. Bui; Resources, C.H. Nguyen; Funding acquisition, V.H. Vu

Data availability statement: Research data is only available upon request

Editor: Marcílio Alves

References

Wang, X., Huang, S., Hong, Y., Xie, M., Yang, Y., Yu, H., Zheng, X., (2025a). Flexural behavior of RC beams strengthened with UHPC reinforced by steel mesh and carbon textile mesh under sustained load. Structures 82:110682.

Mercimek, Ö., Yılmaz, M.C., Akkaya, S.T., Yılmaz, T., Anıl, Ö., Erol, H., Kocaman, İ., (2026). Impact behavior of reinforced concrete slabs strengthened with high-strength mortar-bonded carbon textile-reinforced mortar strips without anchors. Journal of Building Engineering 119:115268.

Silva, R.M.d.C., Silva, F.d.A., (2025). Flexural strengthening efficiency of small-scale RC beams using textile reinforced concrete (TRC) with mineral-impregnated carbon fabrics. Structures 77:109056.

Guo, R., Ren, Y., Shao, J., Xia, M., Pan, Y., (2025). Flexural performance of pre-damaged RC beams under sustained loading strengthened with FRP grid-ECC composite layers. Engineering Structures 343:121201.

Tan, K.H., Saha, M.K., Liew, Y.S., (2009). FRP-strengthened RC beams under sustained loads and weathering. Cement and Concrete Composites 31(5):290–300.

Nerilli, F., Ferracuti, B., (2022). A tension stiffening model for FRCM reinforcements calibrated by means of an extended database. Composite Structures 284:115100.

Sabzi, J., Esfahani, M.R., Ramezani, A., Ozbakkaloglu, T., (2024). A comparison between the behavior of beams strengthened by FRP sheets and FRCM composites. Engineering Structures 306:117796.

Elghazy, M., El Refai, A., Ebead, U., Nanni, A., (2017). Effect of corrosion damage on the flexural performance of RC beams strengthened with FRCM composites. Composite Structures 180:994–1006.

Wang, W., Li, L., Chen, J., Dai, K., (2025b). Experimental and analytical study on flexural behavior of corroded RC beams strengthened with CFRP rods and UHPC. Engineering Structures 323:119299.

Yang, J., Yu, J., Zhang, Z., Zou, Y., Chen, R., Zhou, J., Li, B., (2023). Flexural behavior of 15-year-old full-scale hollow slab beams strengthened with fiber-reinforced composites. Case Studies in Construction Materials 19:e02545.

ACI (2020). ACI 549.4R-20: Guide to Design and Construction of Externally Bonded Fabric-Reinforced Cementitious Matrix and Steel-Reinforced Grout Systems.

CNR (2018). CNR-DT 215/2018: Guide for the Design and Construction of Externally Bonded Fibre Reinforced Inorganic Matrix Systems.

Koutas, L.N., Triantafillou, T.C., (2019). Strengthening of concrete structures with textile reinforced mortars: state-of-the-art review. Journal of Composites for Construction 23(1).

Weiland, S., (2009). Flexural strengthening of RC structures by textile reinforced concrete. PhD Thesis, Technische Universität Dresden.

Bencardino, F., Carloni, C., Condello, A., Realfonzo, R., (2018). Flexural behaviour of RC members strengthened with FRCM: state-of-the-art and predictive formulas. Composites Part B 148:132–148.

Adam, V., Bielak, J., Dommes, C., Will, N., Hegger, J., (2020). Flexural and shear tests on reinforced concrete bridge deck slab segments with a textile-reinforced concrete strengthening layer. Materials 13:4210.

Xie, W., Sheng, J., Yu, Z., Li, Y., Dou, G., (2023). Flexural behavior of corroded RC beams strengthened by textile-reinforced concrete. Buildings 13(12):2902.

Xu S.L., Zhang X.F (2009), Theoretical analysis and experimental investigation on flexural performance of steel reinforced ultrahigh toughness cementitious composite RUHTCC beams, Science in China Series E: Technological Sciences, 2009, 52(4): 1068–1089.

Zulassung Z-31.10-182 (2023) Gegenstand: Verfahren zur Verstärkung von Stahlbeton mit TUDALIT (Textilbewehrter Beton), Prüfstelle: DIBt, Antragsteller: TUDAG TU Dresden Aktiengesellschaft